Stormy Weather in Galaxy Clusters

Jack O. Burns

Recent x-ray, optical, and radio observations coupled with particle and gas dynamics numerical simulations reveal an unexpectedly complex environment within clusters of galaxies, driven by ongoing accretion of matter from large-scale supercluster filaments. Mergers between clusters and continuous infall of dark matter and baryons from the cluster periphery produce long-lived "stormy weather" within the gaseous cluster atmosphere—shocks, turbulence, and winds of more than 1000 kilometers per second. This weather may be responsible for shaping a rich variety of extended radio sources, which in turn act as "barometers" and "anemometers" of cluster weather.

Groups and clusters of galaxies are the largest gravitationally bound and collapsed systems in the universe. A group may contain as few as three galaxies whereas a cluster such as Coma (Fig. 1) may contain thousands of member galaxies (*1*). A cluster has a typical radius of ~2 Mpc (1 pc = 3.1×10^{13} km) and a total mass of 10^{14} to 10^{15} $M_\odot$ (1 $M_\odot$ equals the mass of the sun). Clusters are potentially powerful testbeds of cosmological models. The number density of clusters, their mass distribution function (number of clusters per unit volume per unit mass), and the degree of substructure can constrain Ω_0, the ratio of the mean mass density of the universe to the closure density (*2, 3*). In turn, Ω_0 determines the fate of the universe (*4*).

Galaxy clusters consist of three mass components: visible galaxies, intracluster gas, and so-called dark matter. The galaxies imaged with optical and infrared telescopes contain only ~1% of the total mass in a cluster. There is evidence that the colors of galaxies in clusters have changed over surprisingly short look-back times, with a higher number of blue galaxies (indicative of new, massive star formation) at earlier epochs (*5*). Ground-based telescope and Hubble Space Telescope images suggest that star formation in distant clusters was triggered by tidal interactions between galaxies (*6*), a mild form of which is termed galaxy harassment (*7*).

The second mass component, the intracluster medium (ICM), is composed of a hot (10^7 to 10^8 K), highly ionized, low density (~10^{-3} cm^{-3}) gas that typically makes up 5 to 10% of the total cluster mass (that is, 5 to 10 times the mass of all the galaxies in a cluster). This gas emits x-rays by thermal free-free radiation and spectral-line transitions. The ICM, enriched with heavy elements (~30 to 50% of solar abundance), was produced in stars within galaxies and then stripped or expelled into the ICM. The details of the ICM enrichment are unclear, but one model proposes that explosions of type II supernovae drive winds that blow material out of the galaxies (*8*).

The third component is some form of dark, unseen matter that gravitationally dominates clusters and constitutes up to 90% of the total mass. The presence of this dark matter is revealed by its gravitational effects on luminous matter (that is, gas and galaxies). By assuming that the galaxies, the gas, or both are bound to, and in equilibrium with, the cluster gravitational potential, we can estimate the mass of the dark matter (*9*). Clusters can also act as gravitational lenses which reimage distant galaxies that lie behind them into arcs of diffuse light. The observed curvature and distribution of cluster arcs can then be used to model the cluster's mass distribution. Typically, gravitational lens calculations produce cluster masses that agree to within a factor of ~2 with those estimated from galaxy dynamics and confinement of the gas (*10*).

The fraction of normal baryonic matter in clusters (gas, dust, and stars), based on the above mass components, is inconsistent with that expected from the observed amounts of light elements (H, He, and Li) that formed shortly after the Big Bang in an $\Omega_0 = 1$ universe (*11*). Some of this discrepancy may be caused by errors in the mass estimates, because not all clusters are in virial and hydrostatic equilibrium, or other components such as turbulence and magnetic fields may be important sources of gas pressure (*12*). Most likely, however, this so-called baryon catastrophe suggests that Ω_0 is really <1 (and, hence, the universe is open), which is consistent with other recent measurements (*3*).

A Whole Lot of Shaking Going On

Less than a decade ago, most astronomers believed that galaxy clusters were relatively simple, spherical balls of galaxies and gas that are in equilibrium with the dark matter. More recent optical and x-ray observations demonstrate that many clusters are far from this mature stage of evolution. Instead, dynamically important substructures of galaxies and gas often appear within clusters. Cluster "substructure" has yet to be rigorously defined; however, statistically significant clumps of galaxies or x-ray photons (above that expected from Poisson statistics for a smooth cluster background), or radial variations of centroid positions, ellipticities, and twists in optical or x-ray isophotes are

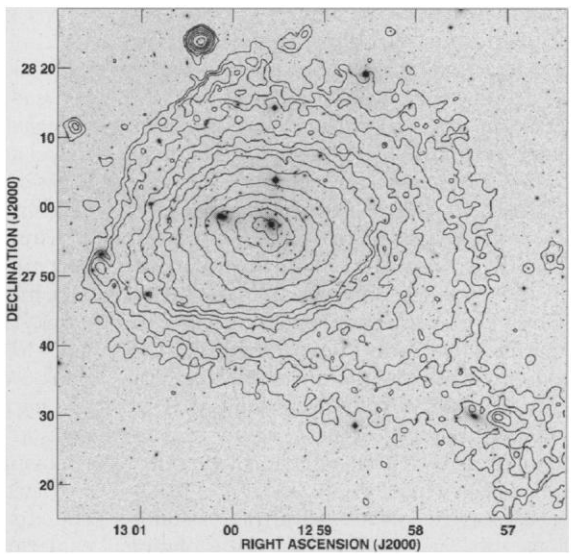

Fig. 1. ROSAT position-sensitive proportional counter x-ray contours of the Coma cluster overlaid onto an optical image from the Palomar Observatory Digital Sky Survey. At a redshift of $z = 0.0232$, 1 arc min corresponds to 27 kpc for $H_0 = 75$ km s^{-1} Mpc^{-1}. The x-ray image was smoothed by a Gaussian beam with full width at half maximum (FWHM) = 1′. The contours (outer to inner) are 0.5, 0.75, 1.0, 1.5, 2, 2.5, 3, 4, 6, 8, 10, 12, and 14×10^{-4} counts s^{-1} (15 arc sec by 15 arc sec pixel)$^{-1}$. The twisting of the x-ray contours between the inner and outer parts of the cluster is reproduced in a numerical model where the galaxy group in the lower right has passed through the core of Coma within the last ~2×10^9 years (2 Gy) (*42*).

The author is at the Office of Research, 205 Jesse Hall, and Department of Physics and Astronomy, University of Missouri, Columbia, MO 65211, USA. E-mail: burns@research.missouri.edu

cited as evidence for substructure (*13*). Depending on the sample selection, 30 to 75% of clusters have substructure (*14, 15*). Even clusters that were once touted as being prototypes of dynamically relaxed systems, such as Coma (Fig. 1), have now been found to have substructure (*16*).

Further evidence for cluster substructures has come with the advent of multifiber spectrographs, with which tens to hundreds of galaxy spectra can be gathered in one telescope pointing. Velocities of hundreds of galaxies per cluster are now routinely measured (*17*). In a cluster that is gravitationally bound and in equilibrium, galaxy velocities have a simple Maxwellian or Gaussian distribution. Deviations from a normal distribution of galaxy velocities [for example, multiple peaks, skewing, or kurtosis (Fig. 2, C and D)] are often cited as evidence for substructure. Optical and infrared images coupled with galaxy spectra can paint an interesting picture of the three-dimensional structure of a cluster. Statistical tests have now been developed to gauge the significance of substructure in the galaxy distribution on the sky and the galaxy velocity distribution (*18*).

After the first systematic x-ray imaging of clusters in the late 1970s with the Einstein Observatory, the Röntgen X-ray Satellite (ROSAT) launched in 1990 has produced hundreds of soft x-ray (0.5 to 2.0 keV) images of groups and clusters (*19*). ROSAT has confirmed that the x-ray surface brightness distributions of many clusters are clumpy and irregular. X-ray substructure is often judged by radial variations in centroid positions, ellipticities, or position angles of x-ray isophotes (*20*). When there is enough signal-to-noise in an image, more sophisticated moment or wavelet analyses of surface brightness can be used to determine if substructure is present (*21*). The Advanced Satellite for Cosmology and Astrophysics (ASCA), with higher resolution spectrometers but relatively poor angular resolution, is producing temperature maps of nearby clusters that show many of them to be nonisothermal and, in some cases, to have spatially asymmetric temperature substructure (*22, 23*). These optical and x-ray telescopes allow us to examine substructure in the galaxies and the gas (Fig. 2). After the application of statistical tests to judge the significance of substructure (*24*), the combined optical and x-ray data allow us to model the evolution of clusters in more detail.

The origin of all these clumps and other apparent substructures observed in galaxy clusters has been addressed through numerical simulations (Fig. 3). These simulations combine particle (*N*-body) techniques, to model the evolution of the dark matter that dominates the gravitational potential, with hydrodynamics, to model the evolution of the x-ray gas (*25*). The gas then responds to the evolving gravitational potential and to fluid dynamical forces such as shock waves and pressure gradients in the ICM. Newly developed adaptive mesh refinement (AMR) codes now achieve spatial dynamic ranges of 8000:1 (ratio of largest to smallest scales of structure), thus allowing us to probe the large- and the small-scale structures in and around clusters (*26*).

The numerical models, which are generally consistent with present observations, show that the universe is composed of a complex web of alternating filaments, sheets or walls, and voids on scales of hundreds of megaparsecs (*27*). The filaments contain baryons and dark matter, whereas the voids are believed to be relatively free of

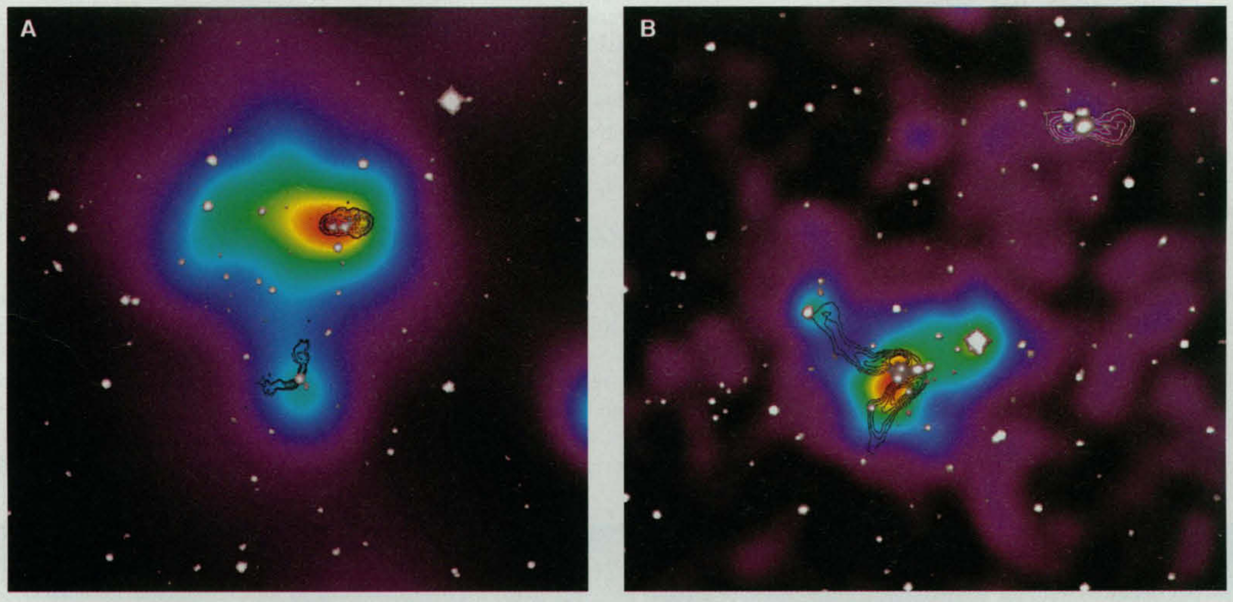

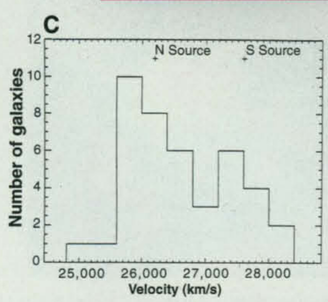

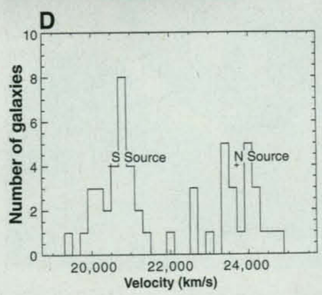

Fig. 2. (**A** and **B**) X-ray, optical, and radio overlays of two clusters that contain substructure correlated with the positions of extended radio sources. The optical fields are from the Digital Sky Survey, the ROSAT x-ray emission is in color, and the contours are VLA radio emission. Each field displays the inner ~25% of the total area of the cluster as defined by Abell *et al.* (*1*). (**C** and **D**) Histograms of the galaxy velocity distributions, which are non-Gaussian and further evidence of recent cluster-cluster mergers. Crosses in (C) and (D) mark velocities of the northern and southern radio sources in (A) and (B). (A) is galaxy cluster Abell 578 (z = 0.09, field size is 920 kpc by 920 kpc), which contains two extended radio sources including a tailed source coincident with a southern extension of resolved x-ray emission; the galaxy velocity distribution is significantly skewed (C). (B) is galaxy cluster Abell 1569 (z = 0.07, field size is 1.10 Mpc by 1.07 Mpc). The northern radio source (white contours) is associated with a group of galaxies offset by ~3000 km s^{-1} from the main cluster (D); the southern tailed radio source shows the strong correlation observed between the position angles of radio tails in WAT sources with elongations in the x-ray (*24, 37*). Both clusters are examples of merging systems where the radio sources act as probes of the resulting disturbed gaseous environs.

matter. Gravitational forces cause initially small density perturbations to collapse into an elaborate network of intersecting filaments (Fig. 3). The cores of galaxy clusters form at the intersections of filaments, while galaxies and stars simultaneously form within clusters. The quasi-spherical clusters grow with time from this hierarchy as gas, galaxies, and dark matter are accreted along filaments and as clusters merge with galaxy groups. Major mergers between clusters probably occur several times (every 2 to 4 Gy) during their evolution (*28*).

The *N*-body and hydrodynamic simulations that focus on the collision of two idealized spherical clusters show some details of the merging process (Fig. 4). Such initial conditions, although simpler than the supercluster environment of real clusters, allow much higher resolution within the cluster cores (20 to 25 kpc) and, thus, better probe the detailed physics of the merger (*29, 30*). Clusters free-fall together with relative velocities of thousands of kilometers per second, which exceeds the sound speed of the ICM. Therefore, the mergers produce shock waves (Mach numbers of 2 to 5) that can result in temperature and density substructures such as those seen in the x-ray data (*31*). Large-scale (tens of kiloparsecs) turbulent eddies and bulk flows of >1000 km s^{-1} can stir the cluster gas for 2 to 5 Gy after the initial passage of the subcluster through the cluster core (Fig. 4). Thus, the gaseous environment within many clusters is far more turbulent and complex than we believed only a few years ago. I characterize this as a kind of "stormy weather" inside clusters.

Radio Galaxies as Cluster Weather Stations

About 10% of galaxies in clusters produce emission at radio wavelengths above a power of 10^{23} W Hz^{-1} at 20 cm (*32*), observable by telescopes such as the Very Large Array (VLA) interferometer. Jets, lobes, and tails of radio-emitting plasma are ejected from galaxy cores (on a parsec-scale) and travel outward, often extending hundreds of kiloparsecs, well beyond the stellar boundaries of the galaxies into the ICM (*33*). This radio plasma is believed to be ~10 to 100 times less dense than the ICM. Radio surveys of clusters from the VLA (*34*) have revealed a rich diversity in structure for the extended radio sources—curved and distorted U-shaped and V-shaped tailed sources, double-lobed sources, and S-shaped morphologies (Fig. 2). The cause of this morphological complexity has been a puzzle for more than two decades.

The low density radio plasma is susceptible to the gas pressure and to pressure gradients in the surrounding ICM (*35*). The internal pressure of the radio source plasma (including pressure components from relativistic electrons, magnetic fields, and hot gas) is believed to be in balance with the thermal pressure [nkT (n is density)] of the cluster gas; otherwise, adiabatic expansion losses would quickly diminish the radio surface brightness and we would see few such extended radio sources. It is likely that the winds, shocks, and general turbulence of the ICM shape the radio sources in complex ways. Injecting radio plasma into this stormy weather environment (Fig. 4) will produce bent and distorted radio sources (as in Fig. 2). Numerical simulations of jets propagating into such cluster gaseous environs evolve extended radio sources that look similar to those seen in clusters (*36*).

There is emerging evidence that extended, low-power, tailed radio sources are most likely to be found in unrelaxed clusters, and this suggests that such radio sources are key probes or even beacons to clusters that have recently experienced accretion events (*15*). Most clusters that contain wide-angle tailed (WAT) radio sources (V-shaped sources with 100- to 1000-kpc-length tails, powered by massive galaxies located at the cluster centers) have optical and x-ray substructure (*37*). In particular, 90% of a statistical sample of WAT clusters has x-ray substructure, principally in the form of asymmetrical extensions between the radio tails (Fig. 2B). Such a correlation between the bending direction of the radio tails and the x-ray elongations is expected from numerical simulations. In these models, cluster-cluster mergers produce a bulk flow along the merger axis with sufficient ram pressure to bend the radio tails and distort the x-ray surface brightness (*29, 30, 35*). A similar trend among a sample of clusters that contain more highly curved, U-shaped, narrow-angle tailed (NAT) radio sources (associated with average brightness, noncentral galaxies) has also been found. About 87% of the NAT clusters show statistically significant x-ray substructure compared with only ~30% for a similar-sized control sample of radio-quiet clusters (*38*). Thus, bent, tailed radio sources appear to prefer unrelaxed clusters. In addition, NAT galaxies have average velocities within clusters, not anomalously high speeds as would have been expected from previous models that predicted that NATs formed from the ram pressure produced by simple galaxy motion through the ICM (*39*). It is the cluster weather, particularly the high winds resulting from recent mergers, that appears to shape the bent jets and tails in the WATs and NATs rather than the motion of the galaxies through a calm ICM. In turn, the radio sources can be used as barometers to measure ICM pressure and as anemometers (*35*) to measure the cluster winds (the only such measure of ICM winds available).

Finally, there is a rare class of cluster radio sources, termed radio halos, that also appear to owe their existence to the evolving gravitational potential and gaseous environs of merging clusters. There are only ~10 well-documented examples of radio halos in rich clusters (*40*), such as that in

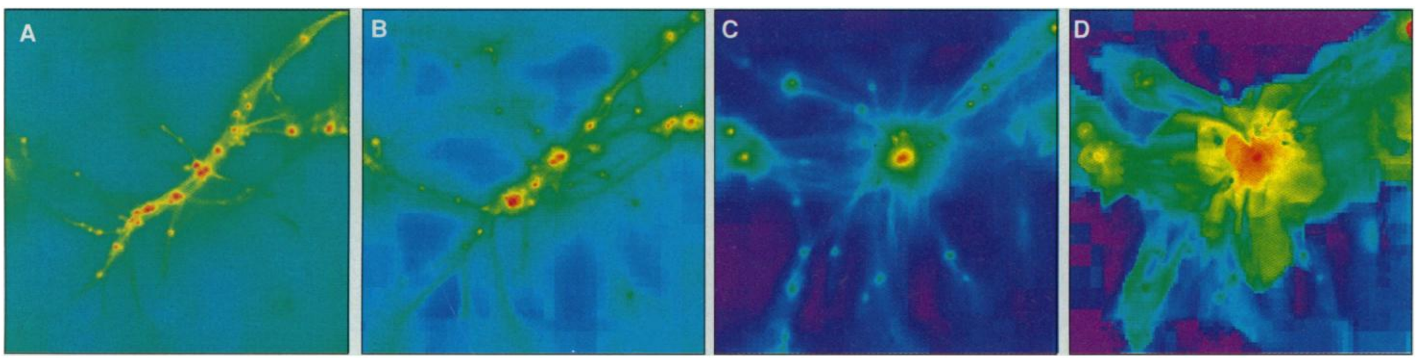

Fig. 3. Evolution of the gas density in a model galaxy cluster from (**A**) a supercluster filament at a redshift of $z = 2$, to (**B**) a more clustered string of galaxy groups at $z = 1$, to (**C**) a quasi-spherical system at the present epoch ($z = 0$), modeled with an AMR *N*-body and hydrodynamics code (*26*). (**D**) Distribution of gas temperature at $z = 0$. Each panel is 16 h^{-1} Mpc on a side ($h = H_0/100$). The grid refinement hierarchy can be seen in (D) where a course grid is used in the outer, lower density regions, whereas higher resolution is needed for the cluster core. Note also the complex temperature substructure in the model.

the Coma cluster, which are not associated with any individual galaxy but rather are amorphous, uncollimated, steep-spectrum sources with diameters up to 2 Mpc (comparable to the cluster size). In all cases examined, these clusters have significant optical or x-ray substructure or both (*23, 41*). In the case of Coma, a numerical model of the effects of a galaxy group passing through the cluster core about 2 Gy ago (*42*) reproduces the unusually high-velocity dispersion of galaxies within the group, and the observed x-ray morphology [including the twisted isophotes near the core and the bridge of x-ray emission between the cluster and the galaxy group (Fig. 1)]. Such a model is also consistent with the positions of poststarburst galaxies (systems with truncated star formation) within the x-ray bridge (*42*). Thus, the radio halo is an equally significant signpost of a merger in the Coma cluster. Because of the megaparsec size of the radio halo, there must be an in situ mechanism within the cluster to re-energize the relativistic electrons initially produced within radio galaxies (*43*) and to amplify initially very weak magnetic fields up to ~2 μG. A merger between the Coma cluster and the group is the only mechanism that appears to have enough energy (~10^{46} ergs s^{-1}) to power the halo (radio luminosity of ~10^{41} ergs s^{-1}). The shock waves and turbulence caused by the group passage could reaccelerate the relativistic electrons distributed throughout the ICM (*44*) and possibly amplify the magnetic fields by a turbulent dynamo process (*45*).

Forecast for the Future

The weather report for galaxy clusters is stormy with alternating high- and low-pressure regions throughout, high winds, turbulence, and heat waves (that is, shock-heating of the cluster atmosphere). With time (billions of years), the weather will calm as the accretion events become more rare; possibly, the occurrence of radio sources within clusters will also diminish with the storms.

An exciting new generation of x-ray satellites, which will markedly improve our understanding of galaxy cluster weather, will be launched over the next 2 to 3 years. NASA's Advanced X-ray Astrophysics Facility (AXAF) will produce greatly improved resolution (0.5 arc sec) of clusters at ~0.5- to 10-keV energies. The European Space Agency's X-ray Multiple Mirror (XMM) telescope will complement AXAF through enhanced spectral resolution to map the distributions of temperatures and elemental abundances across clusters (sensitive probes of the cluster evolutionary state). Finally, the Japanese–United States Astro-E satellite will have the sensitivity and spectral resolution to directly measure wind velocities (by Doppler shifts of spectral lines) within the ICM for the first time.

Numerical particle and hydrodynamics simulations, incorporating adaptive mesh refinement, higher mass resolution, and magnetohydrodynamics, are rapidly advancing along with supercomputer speed and memory. These codes, operating on a new generation of supercomputers, offer the promise of modeling a fair sample of the universe (>50-Mpc-diameter grids) with high spatial fidelity. We can then hope to investigate additional physical processes that may be responsible for producing the complex cluster weather, such as heating of the ICM by an early generation of galaxy supernovae (*46*), and the role of magnetic fields in cluster gas dynamics (*47*).

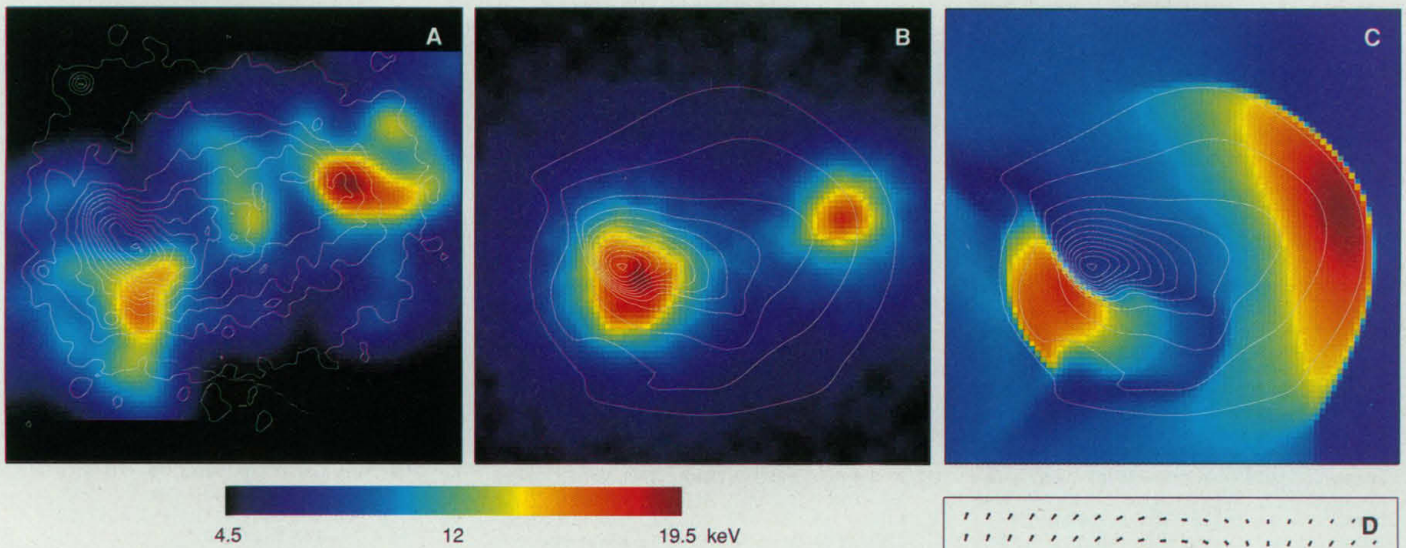

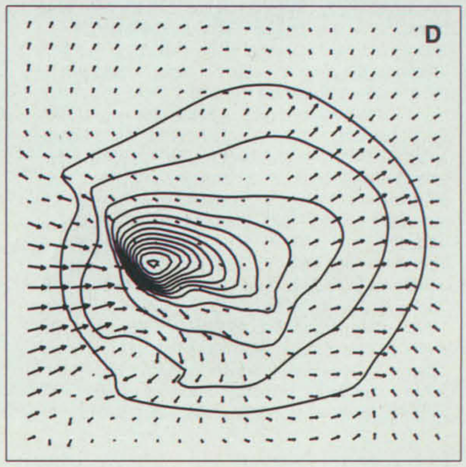

Fig. 4. Optical and x-ray observations of the cluster Abell 754 and numerical simulations that reproduce these observations by using an off-center collision between two galaxy clusters (*49*). (**A**) Observed ROSAT x-ray surface brightness (contours) and projected galaxy densities (colors). For the galaxy distribution, 142 galaxy positions were smoothed with a 40 arc sec FWHM Gaussian. X-ray contour levels are 0.08, 0.16, 0.24, 0.32, 0.4, 0.48, 0.56, 0.64, 0.72, 0.8, 0.9, and 0.99 of the peak. (B), (C), and (D) represent simulated data for a 2.5:1 mass ratio off-center collision 0.3 Gy after closest approach. Each panel is 2 Mpc by 2 Mpc. The smaller of the two clusters (subcluster) entered from the left and is moving to the right. (**B**) Projected dark matter particle distribution (color) and x-ray surface brightness (contours). X-ray contour levels are the same as in (A) except a lower contour at 0.03 of the peak was added. (**C**) Synthetic x-ray surface brightness (contours) and projected x-ray emission–weighted temperature (color with a color bar below the frame). In the temperature image, strong shocks at the peripheries, which have enhanced the temperatures, are visible. (**D**) Gas velocity vectors within the plane of the merger are superposed onto x-ray contours. Vectors are spaced at 100 kpc and scaled to the maximum velocity of 1850 km s^{-1}. Note the high velocities and complex gas velocity patterns at this epoch.

REFERENCES AND NOTES

1. The difference between a group and a cluster of galaxies is not rigorously defined. The division is often based on the Abell catalog [G. O. Abell, H. G. Corwin, R. P. Olowin, *Astrophys. J. Suppl.* **70**, 1 (1989)]. Systems of galaxies with richness class <0 (that is, <30 member galaxies) are usually termed groups, whereas their richer counterparts are called clusters. As defined by Abell *et al.*, richness is a measure of the number of galaxies within a radius of $2h_{75}^{-1}$ Mpc of the cluster center (where $h_{75} = H_0/75$, and H_0 is the Hubble constant).
2. The density parameter Ω_0 is defined as $\rho_0/\rho_c = 8\pi G\rho_0/(3H_0^2)$, where G is the gravitational constant, H_0 is the Hubble constant at the present epoch (75 km s^{-1} Mpc^{-1} is assumed throughout this paper), ρ_0 is the true mass density of the universe, and ρ_c is the critical density (*48*). For $\rho_0 > \rho_c$ ($\Omega_0 > 1$) the universe will collapse into a big crunch, whereas for $\rho_0 < \rho_c$ ($\Omega_0 < 1$) the universe will continue monotonic expansion.
3. The evolution of clusters is driven by mass accretion from large-scale structures. The accretion rate depends on Ω_0 because clusters must form earlier [that is, at larger redshifts or look-back times (*5*)] in a low density universe. Estimates of the density parameter from cluster properties can be found, for example, in D. Richstone, A. Loeb, E. L. Turner, *Astrophys. J.* **393**, 477 (1992); A. Evrard, J. Mohr, D. Fabricant, M. Geller, *Astrophys. J. Lett.* **419**, L9 (1993); N. A. Bahcall, X. Fan, R. Cen, *ibid.* **485**, L53 (1997); J. P. Henry, *ibid.* **489**, L1 (1997); A. E. Evrard, *Mon. Not. R. Astron. Soc.* **292**, 289 (1997).
4. For $\Omega_0 = 1$ (flat universe), the universal expansion rate declines exponentially, but for $\Omega_0 < 1$, the universe is open and will expand forever (*48*).
5. Look-back time, Δt, is defined as the time measured back from the present and is a nonlinear function of the redshift (z) [in (*48*), p. 313]. For Δt = 6 Gy (corresponding to z = 0.9 for H_0 = 75 km s^{-1} Mpc^{-1} and Ω_0 = 0.2), the fraction of blue galaxies is measured to be ~80% of the observed galaxies in each cluster [K. Rakos and J. Schombert, *Astrophys. J.* **439**, 47 (1995)]. This diminishes to ~20% for Δt = 3 Gy (z = 0.4) and ~4% at present [H. Butcher and A. Oemler, *ibid.* **285**, 426 (1984). The trend is generally known as the Butcher-Oemler effect].
6. R. J. Lavery and J. P. Henry, *Astrophys. J.* **330**, 596 (1988); A. Dressler *et al.*, *ibid.* **430**, 107 (1994); W. Couch *et al.*, *ibid.*, p. 121.
7. B. Moore *et al.*, *Nature* **379**, 613 (1996); D. C. Koo *et al.*, *Astrophys. J. Lett.* **478**, 49 (1997).
8. M. Loewenstein and R. Mushotzky, *Astrophys. J.* **466**, 695 (1996).
9. From the velocities of galaxies measured in clusters, the virial theorem (which assumes a bound, self-gravitating system) can be used to estimate the cluster mass such that $M_{VT} = (3\pi/G)\sigma^2 \langle 1/r\rangle^{-1}$, where $\langle 1/r\rangle^{-1}$ is the harmonic radius of the cluster and σ is the line-of-sight velocity dispersion [W. R. Oegerle and J. M. Hill, *Astron. J.* **107**, 857 (1994)]. From x-ray images of ICM free-free emission, the mass needed to gravitationally bind the hot gas can be estimated by assuming that the gas is in hydrostatic equilibrium with the cluster potential such that $M_{HE} = kT(r)r/(G\mu m_p)[-\mathrm{dln}\,\rho(r)/\mathrm{dln}\,r - \mathrm{dln}\,T(r)/\mathrm{dln}\,r]$, where μm_p is the average gas particle mass (0.6 times the proton mass for fully ionized gas), ρ is the gas density, k is the Boltzmann constant, and T is the gas temperature [C. Sarazin, *Rev. Mod. Phys.* **58**, 1 (1986)]. However, the presence of dynamically important substructure in a cluster can produce significant errors in masses estimated with these techniques [(*30*); C. Bird, *Astron. J.* **109**, 920 (1996); C. Balland and A. Blanchard, *ibid.* **487**, 33 (1997)].
10. J. Miralda-Escudé and A. Babul, *Astrophys. J.* **449**, 18 (1995); S. W. Allen, A. C. Fabian, J.-P. Kneib, *Mon. Not. R. Astron. Soc.* **279**, 615 (1996). Unlike the methods discussed in (*9*), mass estimates with gravitational lenses do not require clusters to be free of substructure or in hydrostatic and virial equilibrium.
11. S. D. M. White *et al.*, *Nature* **366**, 429 (1993).
12. A. Loeb and S. Mao, *Astrophys. J.* **435**, 109 (1994).
13. J. J. Mohr, D. G. Fabricant, M. J. Geller, *ibid.* **413**, 492 (1993); J. J. Mohr, A. E. Evrard, D. G. Fabricant, M. J. Geller, *ibid.* **447**, 8 (1995).
14. C. Jones and W. Forman, in *Clusters and Superclusters of Galaxies*, A. Fabian, Ed. (Kluwer, Dordrecht, Netherlands, 1992), pp. 49–70; C. Bird, *Astron. J.* **107**, 1637 (1994).
15. J. O. Burns, G. Rhee, F. Owen, J. Pinkney, *Astrophys. J.* **423**, 94 (1994).
16. S. D. M. White, U. G. Briel, J. P. Henry, *Mon. Not. R. Astron. Soc.* **261**, L18 (1993).
17. Doppler shifts of spectral lines in galaxy spectra are used to measure galaxy velocities. [J. M. Hill and W. R. Oegerle, *Astron. J.* **106**, 831 (1993)].
18. T. C. Beers, K. Flynn, K. Gebhardt, *ibid.* **100**, 32 (1990); J. Pinkney, K. Roettiger, J. O. Burns, C. Bird, *Astrophys. J. Suppl.* **104**, 1 (1996).
19. J. Trümper, *Science* **260**, 1769 (1993); W. Voges, in *Proceedings of the European International Space Year Conference*, T. D. Guyenne and J. J. Hunt, Eds. (ESA, Noordwijk, Netherlands, 1992), p. 9.
20. D. S. Davis and R. F. Mushotzky, *Astron. J.* **105**, 409 (1993).
21. X-ray moment analyses of cluster substructure can be found in papers by D. A. Buote and J. C. Tsai [*Astrophys. J.* **452**, 522 (1995); *ibid.* **458**, 27 (1996)]. An example of the wavelet approach to measure substructure is presented in E. Slezak, F. Durret, D. Gerbal, *Astron. Astrophys.* **108**, 1996 (1994).
22. J. P. Henry and U. G. Briel, *Astrophys. J. Lett.* **443**, L9 (1995); M. Markevitch *et al.*, *ibid.* **436**, L71 (1994).
23. K. Roettiger, J. O. Burns, J. Pinkney, *Astrophys. J.* **453**, 634 (1995).
24. J. Pinkney, J. O. Burns, J. M. Hill, *Astron. J.* **108**, 2031 (1994); P. L. Gómez, M. J. Ledlow, J. O. Burns, J. Pinkney, J. M. Hill, *ibid.* **114**, 1711 (1997).
25. Two approaches have been used to model the gas dynamics in clusters: smooth particle hydrodynamics (SPH) and Eulerian schemes. SPH uses a gridless method similar to *N*-body techniques that affords high spatial dynamic range but less accurate handling of shock waves [A. E. Evrard, *Astrophys. J.* **363**, 349 (1990)]. Eulerian codes use numerical meshes to solve the fluid conservation equations with accurate shock-tracking, but with traditionally lower spatial fidelity [K. Roettiger, C. Loken, J. O. Burns, *Astrophys. J. Suppl.* **109**, 307 (1997); S. Schindler and E. Müller, *Astron. Astrophys.* **272**, 137 (1993)]. This limitation for Eulerian codes is now being overcome with adaptive grid methods (*26*), which use a hierarchy of grid sizes that depend on the density of gas (as in Fig. 3).
26. M. L. Norman, in *Proceedings of the Twelfth Kingston Meeting on Theoretical Astrophysics: Computational Astrophysics*, Astronomical Society of the Pacific (ASP), Halifax, 1997, D. A. Clarke and M. J. West, Eds. (ASP, San Francisco, 1997), p. 363.
27. A. L. Melott *et al.*, *Phys. Rev. Lett.* **51**, 935 (1983); A. L. Melott and S. F. Shandarin, *Astrophys. J.* **410**, 469 (1993).
28. A. C. Fabian and S. J. Daines, *Mon. Not. R. Astron. Soc.* **252**, 17p (1991); A. Edge, A. Stewart, A. C. Fabian, *ibid.* **258**, 177 (1992); C. Loken, A. Klypin, J. Burns, G. Bryan, M. Norman, in preparation.
29. K. Roettiger, J. Burns, C. Loken, *Astrophys. J. Lett.* **407**, L53 (1993).
30. _____, *Astrophys. J.* **473**, 651 (1996).
31. The Rankine-Hugoniot conditions for a compressible gas predict increases in density and temperature across a shock front such that $\rho_2/\rho_1 = (\gamma + 1)M^2/[(\gamma - 1)M^2 + 2]$ and $T_2/T_1 = [2\gamma M^2 - (\gamma - 1)][(\gamma - 1)M^2 + 2]/[(\gamma + 1)M]^2$, where γ is the ratio of specific heats (which is 5/3 for ideal gas in the ICM) and M is the Mach number [S. N. Shore, *An Introduction of Astrophysical Hydrodynamics* (Academic Press, San Diego, CA, 1992), p. 107]. For supersonic mergers between clusters with infall Mach numbers of 2 and 5, the gas density behind the shock increases by factors 2.3 and 3.6 over the ICM before the shock, and the temperature increases by factors of 2.1 and 8.7, respectively. Thus, x-ray surface brightness ($\propto\rho^2T^{1/2}$) and temperature maps will show significant variations (that is, substructure) between regions of shocked and unshocked gas.
32. M. Ledlow, in *The Second Stromlo Symposium: The Nature of Elliptical Galaxies*, M. Arnaboldi, G. S. Da Costa, P. Saha, Eds. (ASP, San Francisco, 1997), vol. 116, p. 421.
33. Ultrarelativistic electrons [with $\gamma = (1 - v^2/c^2)^{-1/2} > 1000$, where v is the electron velocity and c is the speed of light] gyrate within magnetic fields (typically ~10 μG) in the plasma to produce radio emission by synchrotron radiation. [For more details on extended radio sources, see, for example, J. O. Burns, M. L. Norman, D. A. Clarke, *Science* **253**, 522 (1991).]
34. J.-H. Zhao, J. O. Burns, F. N. Owen, *Astron. J.* **98**, 64 (1989); F. N. Owen and M. Ledlow, *Astrophys. J. Suppl.* **108**, 41 (1997).
35. For a laminar fluid jet, the bending of the flow subjected to an external pressure gradient in the form of a wind is described by the time-independent Euler's equation in the form [C. P. O'Dea, *Astrophys. J.* **295**, 80 (1985)] $w_j\gamma^2\beta^2/R = \rho_{ICM}v_{rel}^2/h$, where w_j is the jet relativistic enthalpy per unit volume ($\approx\rho_j v_j^2$ for a cold jet with Mach number $\gg$1), $\beta = v_j/c$, $\gamma = (1 - \beta^2)^{-1/2}$, R is the jet radius of curvature, ρ_{ICM} (ρ_j) is the density of the ICM (jet), v_{rel} (v_j) is the velocity of the surrounding medium relative to the radio galaxy (jet velocity), and h is the scale length over which the ram pressure is exerted (~galaxy radius). For a light jet ($\rho_j/\rho_{ICM} \ll 1$), the collimated plasma flow in U-shaped sources must experience transverse winds with typical velocities of $\gtrsim$1000 km/s to bend to their observed curvature, assuming typical jet and ICM properties. Thus, the observed jet curvature can be used to constrain the relative velocity of the radio source with respect to the surrounding gas.
36. C. Loken *et al.*, *Astrophys. J.* **445**, 80 (1995).
37. P. L. Gómez *et al.*, *ibid.* **474**, 580 (1997); J. Pinkney *et al.*, *ibid.* **416**, 36 (1993).
38. M. Bliton, E. Rizza, J. O. Burns, F. N. Owen, M. Ledlow, *Mon. Not. R. Astron. Soc.*, in press.
39. T. W. Jones and F. N. Owen, *Astrophys. J.* **234**, 818 (1979); M. C. Begelman, M. J. Rees, R. D. Blandford, *Nature* **279**, 770 (1979).
40. R. J. Hanisch, *Astron. J.* **85**, 1565 (1980); K.-T. Kim *et al.*, *Astrophys. J.* **355**, 29 (1990).
41. J. O. Burns *et al.*, *Astrophys. J.* **446**, 583 (1995); P. C. Tribble, *Mon. Not. R. Astron. Soc.* **263**, 31 (1993).
42. J. O. Burns, K. Roettiger, M. Ledlow, A. Klypin, *Astrophys. J. Lett.* **427**, L87 (1994).
43. Relativistic electrons, which are responsible for producing the synchrotron radio emission, cannot travel across the megaparsec-diameter halos within their radiative lifetime, even traveling at velocities of nearly *c*. Thus, some form of in situ reacceleration is required.
44. A Fermi-like mechanism involving shocks or turbulence is most often proposed for in situ reacceleration of electrons [J. A. Eilek and P. E. Hughes, in *Astrophysical Jets*, P. E. Hughes, Ed. (Cambridge Univ. Press, Cambridge, 1990), pp. 428–483].
45. D. S. De Young, *Astrophys. J.* **241**, 81 (1980).
46. R. Cen and J. P. Ostriker, *ibid.* **417**, 404 (1993); A. Evrard, *ibid.* **437**, 564 (1994).
47. K. Roettiger and J. M. Stone, *Bull. Am. Astron. Soc.*, **29**, 1302 (1997).
48. P. J. E. Peebles, *Principles of Physical Cosmology* (Princeton Univ. Press, Princeton, NJ, 1993).
49. K. Roettiger, J. Stone, R. Mushotzky, *Astrophys. J.* **493**, 62 (1998).

50. Supported in part by NSF grants AST-9317596 and AST-9896039 and NASA grant NAGW-3152. I am indebted to my collaborators who contributed to the work described here, including M. Bliton, G. Bryan, P. Gómez, J. Hill, A. Klypin, M. Ledlow, C. Loken, M. Norman, F. Owen, J. Pinkney, E. Rizza, K. Roettiger, W. Voges, and R. A. White. I particularly acknowledge M. Ledlow, P. Gómez, C. Loken, G. Bryan, and K. Roettiger for their help with Figs. 1 through 4. I also thank A. Melott, S. Shandarin, and J. P. Henry for their useful comments on the text.